# Reduction of nitrate to ammonia using photocatalytically accumulated electrons on titanium(IV) oxide in a time-separated redox reaction

Naoya Murakami*, Masato Suenaga, Ryota Deguchi

Graduate School of Life Science and Systems Engineering, Kyushu Institute of Technology, 2-4 Hibikino, Wakamatsu-ku, Kitakyushu 808-0196, Japan

* Corresponding author. TEL: +81-93-695-6038, E-mail address: murakami@life.kyutech.ac.jp

Abstract

Reduction of nitrate ($NO_3^-$) to ammonia ($NH_3$) was performed by a time-separated redox reaction using photocatalytically accumulated electrons in a titanium(IV) oxide ($TiO_2$) suspension. The time-separated redox reaction uses a two-step reaction under the control of photoexcitation and an electron acceptor: (1) accumulation of electrons in $TiO_2$ powder under photoexcitation and (2) reduction of added $NO_3^-$ by accumulated electrons in the dark. Color change of $TiO_2$ depending on the degree of electron accumulation was observed during the reaction, and 8-electron reduction of $NO_3^-$ to $NH_3$ was performed by accumulated electrons. The results of the time-separated redox reaction using 10 kinds of commercial $TiO_2$ powder indicate that the use of a rutile sample with a large number of trivalent titanium species is a key issue for $NH_3$ production.

Keywords: photocatalyst; electron accumulation; titanium(IV) oxide; ammonia

## 1. Introduction

Photocatalytic reactions using semiconductor materials have been intensively studied for chemical energy conversion technology with various applications such as water splitting [1-3], carbon dioxide reduction [4,5], and organic synthesis [6-8]. The reaction is thought to proceed as a result of simultaneous oxidation and reduction by photoexcited electrons and positive holes, respectively. Therefore, the use of appropriate photocatalytic materials and the design of an appropriate reaction system are important for utilization of electrons and positive holes in target reaction. For example, in organic synthesis by photocatalytic reduction, hole scavengers such as alcohol are often used to efficiently obtain the target substance because oxidation of reductive products, i.e., back reaction, easily occurs and it decrease the reaction rate as well as the selectivity.

"Spatial" separation of redox sites is a conventional approach for retarding the back reaction in a photocatalytic system, and it has been performed by co-catalyst loading and/or surface structure control of the photocatalytic material [9-12]. Another plausible way is "time" separation of the redox reaction, and such a reaction has been studied as a reductive energy-storage system using titanium(IV) oxide ($TiO_2$) and tungsten(VI) oxide [13]. Recently, the reaction has been applied to several kinds of reaction such as hydrogenation of carbonyl compounds [14] and reduction of toxic metal ions, nitrate ($NO_3^-$), nitric oxide (NO) or nitrite ($NO_2^-$) [15,16] using $TiO_2$ and hydrogen evolution using carbon nitride [17]. The reaction uses a two-step reaction under the control of photoexcitation and an electron acceptor as shown in Fig.1. In the first step, electron accumulation is induced by photoexcitation in the absence of an electron acceptor as a counterpart of the reaction of positive holes with a scavenger. Subsequently, accumulated electrons react with the electron acceptor, which is added in the second step, in the dark if the accumulated electrons have more negative potential than the redox potential of the acceptor. Here, the important point of the reaction is that only reduction proceeds without oxidation by positive holes, and this means complete inhibition of the back reaction in the second step.

For a metal oxide semiconductor, electron accumulation is induced by electron trapping at a metal

ion with an oxygen vacancy in the semiconductor. For example, a possible structure of electron accumulation in $TiO_2$ is thought to be trivalent titanium ($Ti^{3+}$) species, and it is considered that defective sites can be empirically measured by evaluation of $Ti^{3+}$ [18]. In our recent study, photoacoustic Fourier transform infrared spectroscopy clarified the energy level of $Ti^{3+}$ in $TiO_2$ powder, which was relatively negative depending on the crystal structure [19], and such defects on the semiconductor surface have been studied as active centers for photocatalytic reaction [20,21].

In the present study, reduction of nitrate ($NO_3^-$) to ammonia ($NH_3$) by a time-separated redox reaction using accumulated electrons on $TiO_2$ was studied. The $NO_3^-$ to $NH_3$ process can be applied to production of useful $NH_3$, which can be widely used as fertilizer, fuels, and chemical precursors, from $NO_3^-$ included in agricultural waste water, and electrochemical reduction of $NO_3^-$ to $NH_3$ has been studied [22-28]. Although photocatalytic reduction of $NO_3^-$ to $NH_3$ has also been reported [29-31], it is thought that only conduction band electrons contribute to $NH_3$ production. The reduction of $NO_3^-$ to $NH_3$ proceeds as follows:

$$NO_3^- + 9H^+ + 8e^- = NH_3 + 3H_2O, 1.20\ \text{V vs NHE (pH = 0)} \quad (\text{eq. } 1)$$

This reaction requires 8-electron reduction, but its redox potential is not so negative compared to the energy level of $Ti^{3+}$, as suggested by our group and other groups [18,19]. Therefore, it is thought that some of the accumulated electrons on $TiO_2$ have sufficient negative potential for $NO_3^-$-to-$NH_3$ reduction (eq. 1) to proceed. Actually, a few groups reported reduction of $NO_3^-$ by electrons accumulated in $TiO_2$ particles by ultra-violet (UV) or gamma-ray irradiation, but only limited $TiO_2$ colloid samples were used in the studies [15]. In the present study, $NH_3$ production by time-separated redox reaction was investigated using 10 kinds of commercial $TiO_2$ powder, and it is discussed here from the viewpoint of crystal structure and $Ti^{3+}$ amount as the saturation amount of electron accumulation.

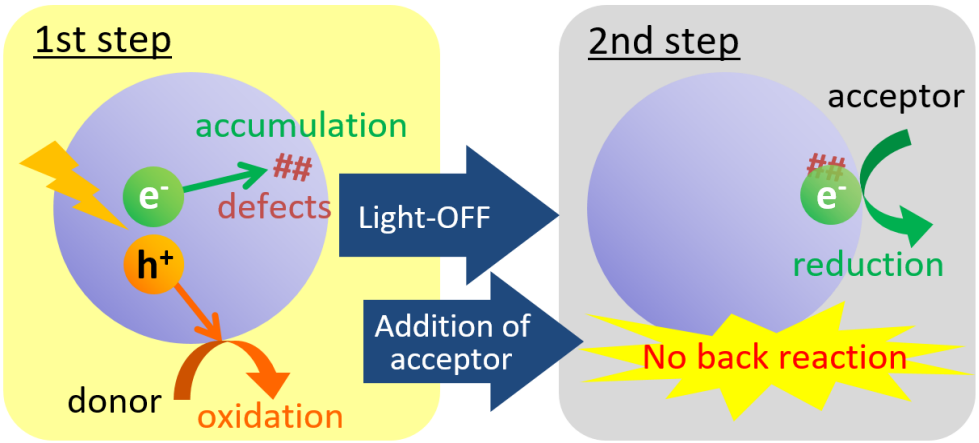


Figure 1. Schematic illustration of the time-separated redox reaction.

## 2. Experimental

### 2.1 Materials

A total of 10 kinds of $TiO_2$ powder samples from commercial sources, including ST-01, ST-41 and CR-EL (Ishihara Sangyo Co.), MT-500B and MT-600B (TAYCA Co.), and reference catalysts JRC-TIO-1, JRC-TIO-6, JRC-TIO-12, JRC-TIO-13 and JRC-TIO-15 supplied by the Catalysis Society of Japan, were used. Before evaluation of the photocatalytic activity, aqueous suspensions containing each $TiO_2$ sample were photoirradiated with a UV light-emitting diode (Nichia, NCU133B), which emitted light at a wavelength of ca. 365 nm, under aerated conditions and they were washed with deionized water several times in order to remove organic compounds in the samples. Other analytical-grade reagents were used without further purification.

### 2.2 Photocatalytic reaction

Fifty milligrams of $TiO_2$, 5 mL of 10 vo% 2-propanol, and a PTFE-coated magnetic stirring bar were added to a test tube, and the suspension was treated by ultrasound for 5 min. Air was purged off from the system by passing argon (Ar) through the suspension for 10 min, and then the test tube was sealed with a double-capped rubber septum and a sheet of Parafilm.

In the case of conventional reaction, 100 μL of a 1.0 mmol $L^{-1}$ $KNO_3$ aqueous solution saturated

with Ar was added to the test tube by using a syringe and then the test tube was photoirradiated with a UV light-emitting diode (Nichia, NCSU033B), which emitted light at a wavelength of ca. 365 nm and an intensity of 10 mW $cm^{-2}$, under magnetic stirring. After 24 h of photoirradiation, the resulting suspension was sampled and centrifuged, and then the concentration of $NH_3$ in the supernatant was analyzed by using indophenol blue colorimetry at an absorbance wavelength of 630 nm with a UV-VIS spectrometer (Shimadzu, UV-1800) and LabAssay Ammonia (Wako Pure Chemical Corp.).

In the case of time-separated redox reaction, a test tube containing no $KNO_3$ aqueous solution was photoirradiated for 24 h under magnetic stirring. After 24 h of photoirradiation, 100 μL of a 1.0 mmol $L^{-1}$ $KNO_3$ aqueous solution saturated with Ar was added to the test tube by using a syringe, and the suspension was stirred for a certain time in the dark. After the reaction, the resulting suspension was sampled and centrifuged, and then the concentration of $NH_3$ in the supernatant was analyzed in the same manner as described above. Moreover, the amount of residual $NO_3^-$ was determined by a colorimetric method with a UV-VIS spectrometer (Shimadzu, UV-1800), PACKTEST WAK-NO3 and pretreatment reagent NO3-RA (Kyoritsu Chemical-Check Lab. Corp.).

## 3. Results and discussion

### 3.1. Color change of $TiO_2$ suspension

Figure 2 shows a photograph of a test tube during the time-separated redox reaction. The color of the suspension was white before UV irradiation (Fig. 2a). UV irradiation induced a change in the color of the suspension, and a blue color was clearly observed after 24 h of irradiation (Fig. 2b), but further change in the color was not observed with photoirradiation for more than 24 h. The color recovered as a function of time after $KNO_3$ injection, though a blue color slightly remained (Fig. 3b). These results indicate that the color change is due to accumulation of electrons and that some of the electrons were consumed by the addition of $KNO_3$.

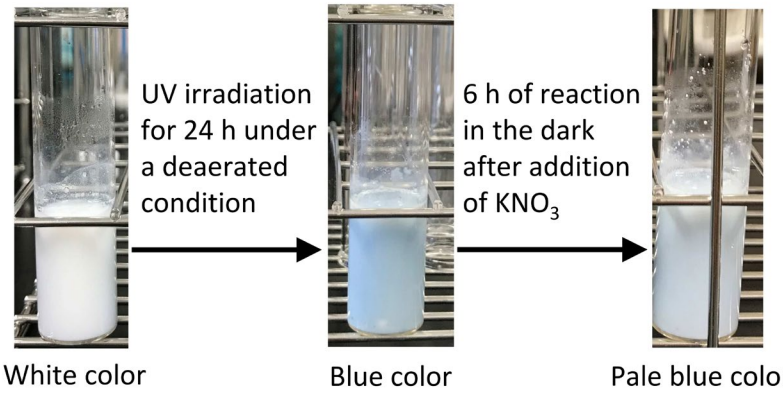


Figure 2. Photographs of a test tube during the time-separated redox reaction.

3.2. Time course of $NH_3$ production

Figure 3 shows the time courses of $NH_3$ production by conventional and time-separated redox reactions. It should be noted that reaction time was defined as not photoirradiation time but time after $KNO_3$ addition. In both types of reaction, $NH_3$ production was increased with an increase in reaction time and showed a tendency for saturation at 100 nmol of $NH_3$ production due to the 100% conversion limit. In contrast, $NH_3$ production was hardly observed in the control experiment (without UV irradiation and without $KNO_3$ addition). These results indicate that the reduction of $NO_3^-$ to $NH_3$ proceeded by accumulated electrons in the time-separated redox reaction. Moreover, the time-separated redox reaction was completed in a few hours, and it was faster than the conventional reaction. The reason for this might be that the numbers of accumulated electrons were 9.5-times larger than the minimum number of electrons required for complete $NO_3^-$-to-$NH_3$ reduction in the case of JRC-TiO-6, which has 152 μmol $g^{-1}$ of $Ti^{3+}$. A slight excess of $NH_3$ production was observed with longer reaction time, presumably due to leakage of air into the reactor at the time of $KNO_3$ injection because it has been reported that nitrogen ($N_2$) gas was photocatalytically converted into $NH_3$ over a rutile $TiO_2$ sample [32].

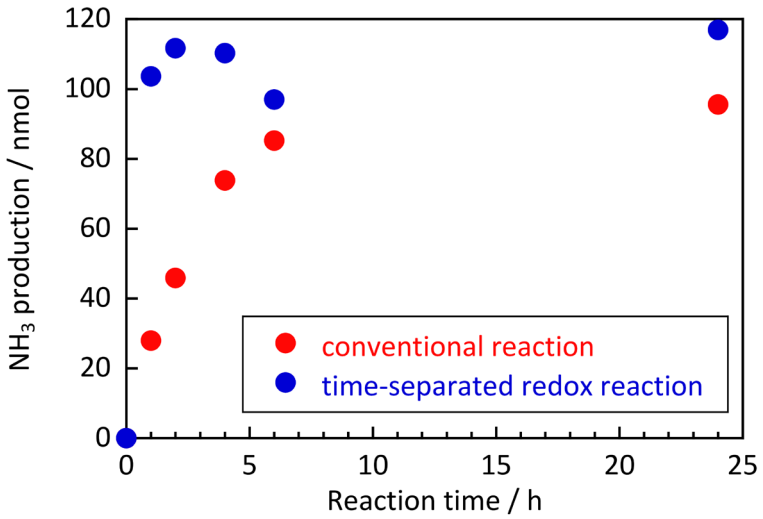


Figure 3. Time courses of $NH_3$ production by conventional and time-separated redox reactions over JRC-TIO-6. Red circles and blue circles show conventional reaction and time-separated redox reaction, respectively.

3.3. Relationships between $NH_3$ production and physical and chemical properties of $TiO_2$ samples

$NH_3$ production and physical and chemical properties $TiO_2$ samples are summarized in Table 1, and Figure 4 shows $NH_3$ production as a function of the amount of $Ti^{3+}$. In the conventional reaction, a linear relationship between $NH_3$ production and $Ti^{3+}$ amount was observed regardless of the crystal structure (Fig. 4a). This agrees with the results of a previous study showing that $Ti^{3+}$ sites work as active sites for $NO_3^-$-to-$NH_3$ reduction [31]. A similar positive correlation was observed between $NH_3$ production and specific surface area. This is a reasonable result because $Ti^{3+}$ sites exist on the surface rather than in the bulk and because $TiO_2$ samples with a larger specific surface area possess a larger $Ti^{3+}$ amount. In contrast, only a rutile sample showed a monotonic increase in $NH_3$ production with increase in the amount of $Ti^{3+}$ in the time-separated redox reaction, and $NH_3$ production using anatase was less than expected (Fig. 4b). However, a proportional relationship between residual $NO_3^-$ and $Ti^{3+}$ amount was observed regardless of the crystal structure (Fig. 5). These results indicate that the kind of reduction by accumulated electrons in $Ti^{3+}$ sites depends on crystal structure, and the deviation from the expected values in Fig. 4b is possibly caused by $NO_3^-$-to-$N_2$ reduction in the anatase

surface as follows:

$$NO_3^- + 6H^+ + 5e^- = \frac{1}{2}N_2 + 3H_2O, +1.25\ \text{V vs NHE (pH = 0)}\ \ (\text{eq. 2})$$

Thus, this reaction (eq. 2) requires a smaller number and a more negative potential of electrons than those required for $NO_3^-$-to-$NH_3$ reduction (eq. 1). Therefore, thermodynamics suggests that $NO_3^-$-to-$N_2$ reduction (eq. 2) proceeds more favorably than $NO_3^-$-to-$NH_3$ reduction if the amount of electrons in the system is limited as in the time-separated redox reaction. On the other hand, continuous supply of electrons from the conduction band possibly induces $NO_3^-$-to-$NH_3$ reduction (eq. 1) in the conventional reaction. Another possible reason is the different surface structures of anatase and rutile samples because the adsorption properties of $NO_3^-$ and its intermediate species on the surface structure of $TiO_2$ have a large influence on the reaction mechanism. A previous study showed that defective sites, i.e., $Ti^{3+}$ sites, work as $NO_3^-$-to-$NH_3$ reduction sites, while Lewis acid sites, which were often observed in the anatase surface, promote nonselective reduction among $N_2$ and $NH_3$ production [35]. For $NO_3^-$-to-$NH_3$ reduction, 8-electron reduction has been reported to proceed via formation of intermediates such as nitrite anion ($NO_2^-$) and nitrogen monoxide (NO) [37] as follows:

$$NO_3^- \xrightarrow{2e^-,2H^+} NO_2^- \xrightarrow{e^-,2H^+} NO \xrightarrow{5e^-,5H^+} NH_3\ \ (\text{eq. 3})$$

The total amount of produced $NH_3$ and residual $NO_3^-$ was almost 100 nmol in almost samples (Table 1), indicating that intermediates were hardly liberated from the surface. Thus, 8-electron reduction proceeded with strong adsorption of intermediate species on the surface, resulting in high selectivity of $N_2$-to-$NH_3$ reduction. On the other hand, the total amount of produced $NH_3$ and residual $NO_3^-$ was significantly less than 100 nmol for some samples (JRC-TIO-13 and JRC-TIO-15). This is because $N_2$ is produced by the reaction between the liberated $NO_2^-$ and other intermediates, such as $NO_2^-$ or NO, followed by reduction of dinitrogen monoxide ($N_2O$) [35].

Although $NH_3$ can be produced from $N_2$ as shown in eq. 4, this $N_2$-to-$NH_3$ reduction requires a more negative potential than those required for the reactions shown eq. 1 and eq. 2.

$$\frac{1}{2}N_2 + 3H^+ + 3e^- = \frac{1}{2}NH_3, +0.55\ \text{V vs NHE (pH = 0)}\ \ (\text{eq. 4})$$

Moreover, it has been shown that anatase is less active than rutile for the reaction of $N_2$-to-$NH_3$ reduction (eq. 4) [32]. Therefore, it is thought that $N_2$-to-$NH_3$ reduction is difficult and that most of the $N_2$ produced remains in the reaction system in the case of an anatase sample.

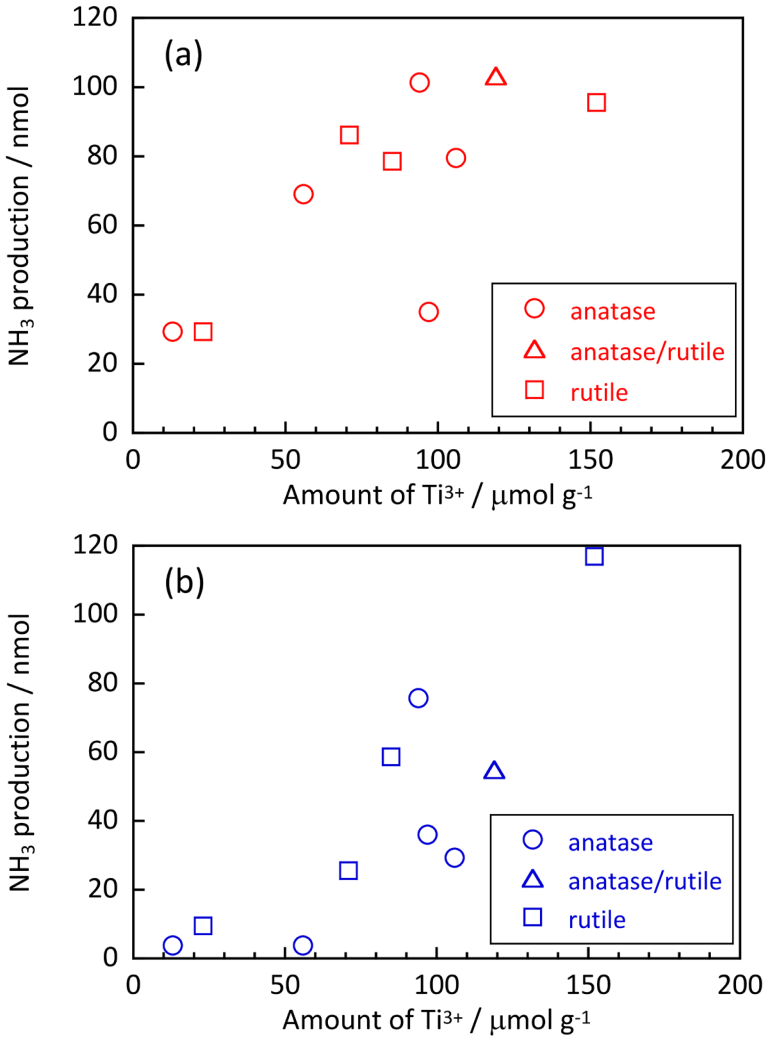


Figure 4. $NH_3$ production in (a) conventional reaction and (b) time-separated redox reaction as a function of amount of $Ti^{3+}$.

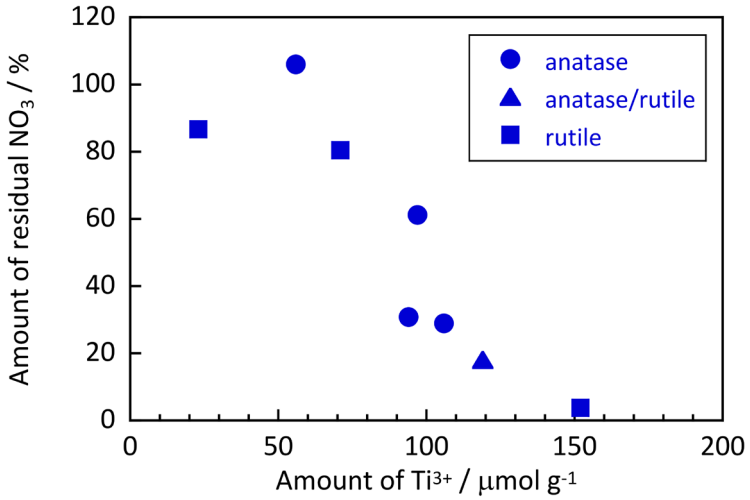


Figure 5. Amount of residual $NO_3^-$ in time-separated redox reaction as a function of amount of $Ti^{3+}$.

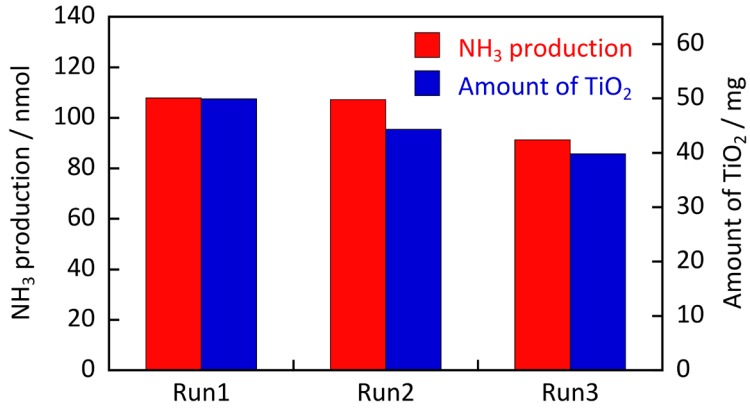


Figure 6. Recycling test in time-separated redox reaction over JRC-TIO-6.

In order to check the stability of the $TiO_2$ sample, time-separated redox reaction was examined by a recycling test three times. Figure 6 shows the results of the recycling test in time-separated redox reaction over JRC-TIO-6. A slight decrease in $NH_3$ production was observed because the amount of $TiO_2$ used in the reaction was also decreased due to some loss in the washing treatment after the reaction. Therefore, photocatalytic activity is possibly stable, taking the amount of $TiO_2$ into consideration. Moreover, the results for the stability and color recovery of $TiO_2$ indicate that the valence of Ti before and after the reactions did not change.

Table 1. $NH_3$ production by and physical and chemical properties of $TiO_2$ samples used in the present study. a) A, R and A/R denote pure anatase, pure rutile and a mixture of anatase and rutile as the crystal structure, respectively (ref. 33, 34 and 35). b) Specific surface areas reported in ref. 33, 34 and 35. c) $Ti^{3+}$ amount reported in ref. 33, and $Ti^{3+}$ amounts in MT-500B and MT-600B were measured by a photoacoustic spectroscopic study (ref. 36). d) Reaction time is 24 h under UV irradiation. e) Reaction time is 24 h in the dark after 24 h of UV irradiation. f) Amount of residual $NO_3^-$ after time-separated reaction.

| Name | [a]Crystal Structure | [b]*S* / $m^2\ g^{-1}$ | [c]$Ti^{3+}$ amount / $\mu mol\ g^{-1}$ | [d]conventional $NH_3$/ nmol | [e]time-separated $NH_3$/ nmol | [f]$NO_3^-$/ nmol |
|---|---|---|---|---|---|---|
| ST-41 | A | 11 | 13 | 29.3 | 3.8 | − |
| JRC-TIO-1 | A | 79 | 97 | 35.0 | 36.0 | 61.2 |
| JRC-TIO-13 | A | 70 | 106 | 79.5 | 29.3 | 28.9 |
| JRC-TIO-12 | A | 359 | 56 | 69.1 | 3.8 | 106 |
| ST-01 | A | 344 | 94 | 101.3 | 75.7 | 30.8 |
| JRC-TIO-15 | A/R | 53 | 119 | 103.2 | 54.9 | 18.0 |
| CR-EL | R | 8 | 23 | 29.3 | 9.5 | 86.7 |
| MT-600B | R | 27 | 71 | 86.1 | 25.6 | 80.5 |
| MT-500B | R | 35 | 85 | 78.6 | 58.7 | − |
| JRC-TIO-6 | R | 102 | 152 | 95.6 | 116.9 | 3.8 |

## 4. Conclusion

In the present study, we firstly showed the reduction process of $NO_3^-$ to $NH_3$ by photocatalytically accumulated electrons in a $TiO_2$ suspension. Although the time-separated redox reaction in the present study could not show sufficient advantages over the conventional method, it can be applied to other kinds of photocatalytic reductive process with no back reaction process. Moreover, the process using the time-separated redox reaction as well as the green ammonia process [38-40] may be an alternative to the Haber-Bosch process.

## CRediT authorship contribution statement

Naoya Murakami: Conceptualization, Writing review & editing, Supervision, Project administration.
Masato Suenaga: Conceptualization, Methodology, Investigation, Writing review & editing.
Ryota Deguchi: Conceptualization, Methodology, Investigation, Writing review & editing.

## Declaration of Competing Interest

The authors declare that they have no known competing financial interests or personal relationships that could have appeared to influence the work reported in this paper.

## Acknowledgements

This work was supported by Grant-in-Aid for Scientific Research(B) (Grant Number 20H02847), Grant-in-Aid for Scientific Research(C) (Grant Number 20K05666) and Grant-in-Aid for Scientific Research on Innovative Areas “Innovations for Light-Energy Conversion (I4LEC)” (Grant Number 20H05107).

## References

[1] T. Takata, J. Jiang, Y. Sakata, M. Nakabayashi, N. Shibata, V. Nandal, K. Seki, T. Hisatomi, K. Domen, Photocatalytic water splitting with a quantum efficiency of almost unity, Nature, 581 (2020) 411–414.

[2] C. Hsu, K. Awaya, M. Tsushida, T. Miyano, M. Koinuma, S. Ida, Water splitting using a photocatalyst with single-atom reaction sites, J. Phys. Chem. C, 124 (2020) 20846–20853.

[3] K. Ogawa, H. Suzuki, C. Zhong, R. Sakamoto, O. Tomita, A. Saeki, H. Kageyama, R. Abe, Layered perovskite oxyiodide with narrow bandgap and long lifetime carriers for water splitting photocatalysis, J. Am. Chem. Soc., 143 (2021) 8446–8453,

[4] S. Yoshino, K. Sato, Y. Yamaguchi, A. Iwase, A. Kudo, Z-schematic $CO_2$ reduction to CO through interparticle electron transfer between $SrTiO_3$:Rh of a reducing photocatalyst and $BiVO_4$ of a water oxidation photocatalyst under visible light, ACS Appl. Energ. Mater., 3 (2020) 10001–10007.

[5] K. Muraoka, M. Eguchi, O. Ishitani, F. Cheviré, K. Maeda, Selective $CO_2$ reduction into formate using Ln-Ta oxynitrides combined with a binuclear Ru(II) complex under visible light, J. Energy Chem., 55 (2021) 176–182.

[6] S. Park, J. Jeong, K. Fujita, A. Yamamoto, H. Yoshida, Anti-Markovnikov hydroamination of alkenes with aqueous ammonia by metal-loaded titanium oxide photocatalyst, J. Am. Chem. Soc., 142 (2020) 12708-12714.

[7] S. Araki, K. Nakanishi, A. Tanaka, H. Kominami, A ruthenium and palladium bimetallic system superior to a rhodium co-catalyst for $TiO_2$-photocatalyzed ring hydrogenation of aniline to cyclohexylamine, J. Catal., 389 (2020) 212–217

[8] M. Fukui, A. Tanaka, H. Kominami, Deoxygenation of pyridine N-oxides in water at room temperature using $TiO_2$ photocatalyst and oxalic acid as a clean hydrogen source, Ind. Eng. Chem. Res., 59 (2020) 11412–11418.

[9] A. Kudo, A. Tanaka, K. Domen, K. Maruya, K. Aika, T. Onishi, Photocatalytic decomposition of water over NiO-$K_4Nb_6O_{17}$ catalyst, J. Catal., 111 (1988) 67–76.

[10] H. Kato, K. Asakura, A. Kudo, Highly efficient water splitting into $H_2$ and $O_2$ over lanthanum-doped $NaTaO_3$ photocatalysts with high crystallinity and surface nanostructure, J. Am. Chem. Soc., 125 (2003) 3082–3089.

[11] T. Ohno, K. Sarukawa, M. Matsumura, Crystal faces of rutile and anatase $TiO_2$ particles and their roles in photocatalytic reactions, New J. Chem., 26 (2002) 1167–1170.

[12] N. Murakami, S. Kawakami, T. Tsubota, T. Ohno, Dependence of photocatalytic activity on particle size of a shape-controlled anatase titanium(IV) oxide nanocrystal, J. Mol. Catal. A: Chem., 358 (2012) 106–111.

[13] T. Tatsuma, S. Saitoh, Y. Ohko, A. Fujishima, $TiO_2$-$WO_3$ photoelectrochemical anticorrosion system with an energy storage ability, Chem. Mater., 13 (2001) 2838–2842.

[14] S. Kohtani, T. Kurokawa, E. Yoshioka, H. Miyabe, Photoreductive transformation of fluorinated acetophenone derivatives on titanium dioxide: defluorination vs. reduction of carbonyl group, Appl.

Catal. A: Gen., 521 (2016) 68–74.

[15] H.H. Mohamed, C.B. Mendive, R. Dillert, D.W. Bahnemann, Kinetic and mechanistic investigations of multielectron transfer reactions induced by stored electrons in $TiO_2$ nanoparticles: A stopped flow study, J. Phys. Chem. A, 115 (2011) 2139–2147.

[16] I.K. Levy, M.A. Brusa, M.E. Aguirre, G Custo, E.S. Román, M.I. Littera, M.A. Grela, Exploiting electron storage in $TiO_2$ nanoparticles for dark reduction of As(V) by accumulated electrons, Phys. Chem. Chem. Phys., 15 (2013) 10335–10338.

[17] V.W. Lau, D. Klose, H. Kasap, F. Podjaski, M. Pigni, E. Reisner, G. Jeschke, B.V. Lotsch, Dark Photocatalysis: Storage of solar energy in carbon nitride for time-delayed hydrogen generation, Angew. Chem. Int. Ed., 56 (2017) 510–514.

[18] S. Ikeda, N. Sugiyam, S. Murakami, H. Kominami, Y. Kera, H. Noguchi, K. Uosaki, T. Torimoto, B. Ohtani, Quantitative analysis of defective sites in titanium(IV) oxide photocatalyst powders, Phys. Chem. Chem. Phys., 5 (2003) 778–783.

[19] T. Shinoda, N. Murakami, Photoacoustic Fourier transform near- and mid-infrared spectroscopy for measurement of energy levels of electron trapping sites in titanium(IV) oxide photocatalyst powders, J. Phys. Chem. C,123 (2019) 12169–12175.

[20] J. Wang, Y. Sun, L. Fu, Z. Sun, M. Ou, S. Zhao, Y. Chen, F. Yu, Y. Wu, A defective g-$C_3N_4$/RGO/$TiO_2$ composite from hydrogen treatment for enhanced visible-light photocatalytic $H_2$ production, Nanoscale, 12 (2020) 22030–22035.

[21] X. Chen, J. Zhao, G. Li, D. Zhang, H. Li, Recent advances in photocatalytic renewable energy production, Energy Mater. 2 (2022) 200001.

[22] Z. Li, G. Wen, J. Liang, T. Li, Y. Luo, Q. Kong, X. Shi, A.M. Asiri, Q. Liu, X. Sun, High-efficiency nitrate electroreduction to ammonia on electrodeposited cobalt–phosphorus alloy film, Chem. Commun., 57 (2021) 9720–9723.

[23] X. Fan, L. Xie, J. Liang, Y. Ren, L. Zhang, L. Yue, T. Li, Y. Luo, N. Li, B. Tang, Y. Liu, S. Gao, A.A. Alshehri, Q. Liu, Q. Kong, X. Sun, In situ grown $Fe_3O_4$ particle on stainless steel: A highly

efficient electrocatalyst for nitrate reduction to ammonia, Nano Res. 15 (2021) 3050–3055.

[24] Z. Deng, J. Liang, Q. Liu, C. Ma, L. Xie, L. Yue, Y. Ren, T. Li, Y. Luo, N. Li, B. Tang, A.A. Alshehri, I. Shakir, P.O. Agboola, S. Yan, B. Zheng, J. Du, Q. Kong, X. Sun, High-efficiency ammonia electrosynthesis on self-supported $Co_2AlO_4$ nanoarray in neutral media by selective reduction of nitrate, Chem. Eng. J., 435 (2022) 135104.

[25] Q. Liu, L. Xie, J. Liang, Y. Ren, Y. Wang, L. Zhang, L. Yue, T. Li, Y. Luo, N. Li, B. Tang, Y. Liu, S. Gao, A.A. Alshehri, I. Shakir, P.O. Agboola, Q. Kong, Q. Wang, D. Ma, X. Sun, Ambient Ammonia Synthesis via Electrochemical Reduction of Nitrate Enabled by $NiCo_2O_4$ Nanowire Array, Small, 18 (2022) 2106961.

[26] Z. Li, J. Liang, Q. Liu, L. Xie, L. Zhang, Y. Ren, L. Yue, N. Li, B. Tang, A.A. Alshehri, M.S. Hamdy, Y. Luo, Q. Kong, X. Sun, High-efficiency ammonia electrosynthesis via selective reduction of nitrate on $ZnCo_2O_4$ nanosheet array, Mater. Today Phys., 23 (2022) 100619.

[27] Q. Chen, X. An, Q. Liu, X. Wu, L. Xie, J. Zhang, W. Yao, M.S. Hamdy, Q. Kong, X. Sun, Boosting electrochemical nitrite–ammonia conversion properties by a Cu foam@$Cu_2O$ catalyst, Chem. Commun., 58 (2021) 517–520.

[28] D. Zhao, J. Liang, J. Li, L. Zhang, K. Dong, L. Yue, Y. Luo, Y. Ren, Q. Liu, M.S. Hamdy, Q. Li, Q. Kong, X. Sun, A $TiO_{2-x}$ nanobelt array with oxygen vacancies: an efficient electrocatalyst toward nitrite conversion to ammonia, Chem. Commun., 58 (2022) 3669–3672.

[29] A. Kudo, K. Domen, K. Maruya, T. Onishi, Photocatalytic reduction of $NO_3^-$ to form $NH_3$ over Pt-$TiO_2$, Chem. Lett., 16 (1987) 1019–1022.

[30] H. Kominami, A. Furusho, S. Murakami, H. Inoue, Y. Kera, B. Ohtani, Effective photocatalytic reduction of nitrate to ammonia in an aqueous suspension of metal-loaded titanium(IV) oxide particles in the presence of oxalic acid, Catal. Lett., 76 (2001) 31−34.

[31] H. Hirakawa, M. Hashimoto, Y. Shiraishi, T. Hirai, Selective nitrate-to-ammonia transformation on surface defects of titanium dioxide photocatalysts, ACS Catal., 7 (2017) 3713−3720.

[32] H. Hirakawa, M. Hashimoto, Y. Shiraishi, T. Hirai, Photocatalytic conversion of nitrogen to

ammonia with water on surface oxygen vacancies of titanium dioxide, J. Am. Chem. Soc., 139 (2017) 10929−10936.

[33] A. Nitta, M. Takashima, M. Takase, B. Ohtani, Identification and characterization of titania photocatalyst powders using their energy-resolved distribution of electron traps as a fingerprint, Catal. Tod., 321 (2019) 2–8.

[34] N. Murakami, T. Chiyoya, T. Tsubota, T. Ohno, Switching Redox Site of Photocatalytic Reaction on Titanium(IV) Oxide Particles Modified with Transition Metal Ion Controlled by Irradiation Wavelength, Appl. Catal. A: Gen., 348 (2008) 148–152.

[35] T. Tanabe, W. Miyazawa, T. Gunji, M. Hashimoto, S. Kaneko, T. Nozawa, M. Miyauchi, F. Matsumoto, Site-selective deposition of binary Pt-Pb alloy nanoparticles on $TiO_2$ nanorod for acetic acid oxidative decomposition, J. Catal., 340 (2016) 276–286.

[36] N. Murakami, O.O.P. Mahaney, R. Abe, T. Torimoto, B. Ohtani, Double-beam photoacoustic spectroscopic studies on transient absorption of titanium(IV) oxide photocatalyst powders, J. Phys. Chem., C, 111 (2007) 11927–11935.

[37] R. Zhang, D. Shuai, K.A. Guy, J.R. Shapley, T.J. Strathmann, C.J. Werth, Elucidation of Nitrate Reduction Mechanisms on a Pd-In Bimetallic Catalyst using Isotope Labeled Nitrogen Species, ChemCatChem, 5 (2013, 5) 313−321.

[38] T. Haruyama, T. Namise, N. Shimoshimizu, S. Uemura, Y. Takatsuji, M. Hino, R. Yamasaki, T. Kamachi, M. Kohno, Non-catalyzed one-step synthesis of ammonia from atmospheric air and water, Green Chem., 18 (2016) 4536–4541 (2016).

[39] B.H.R. Suryanto, H. Du, D. Wang, J. Chen, A.N. Simonov, D.R. MacFarlane, Challenges and prospects in the catalysis of electroreduction of nitrogen to ammonia, Nat. Catal., 2 (2019) 290–296.

[40] T. Ye, S. Park, Y. Lu, J. Li, J. Wu, M. Sasase, M. Kitano, H. Hosono, Dissociative and associative concerted mechanism for ammonia synthesis over Co-based catalyst, J. Am. Chem. Soc., 143 (2021) 12857–12866 (2021).